



# The Effect of Heat Treatments on the Microstructural Evolution of Twin-Roll-Cast Al-Fe-Si Alloys

Jieke Ren, Xiaoyang Fang, Dengbin Chen, Cheng Cao, Youwei He, and Jiabin Liu

Submitted: 14 August 2020 / Revised: 16 February 2021 / Accepted: 27 March 2021 / Published online: 19 April 2021

Dilute Al-Fe-Si alloys with different Fe-Si ratios were prepared by twin-roll casting, rolling and heat treatment. Tensile measurements, optical microscopic observations and electron microscopy observations were performed to investigate the effects of heat treatments on the properties and microstructure evolution of the Al-Fe-Si alloys. The results indicate that in twin-roll cast dilute Al-Fe-Si alloys, the  $\beta$ -AlFeSi,  $\alpha_c$ -Al<sub>12</sub>Fe<sub>3</sub>Si and  $\alpha'$ -Al<sub>8</sub>Fe<sub>2</sub>Si phases coexist. Eutectic  $\alpha_c$ -Al<sub>12</sub>Fe<sub>3</sub>Si can be observed due to the higher Fe concentration in the center layer. In a twin-roll cast Al-0.36Fe-0.4Si alloy, annealing at temperatures of 400 °C or higher would lead to the refinement of intermetallic particles, which is due to the partial dissolution of intermetallic particles or the decomposition of Si-rich phases. During a slow cooling period after annealing, the coarsening of the  $\alpha'$ -Al<sub>8</sub>Fe<sub>2</sub>Si phase occurred below 400 °C after partial dissolution. The recrystallized grain size is not obviously affected by the evolution of intermetallic phases. The morphologies and types of intermetallic phases in twin-roll cast Al-0.44Fe-0.24Si alloy are unaffected by the heat treatments.

**Keywords** 1XXX aluminum, Al-Fe-Si phases, heat treatment, twin-roll casting

## 1. Introduction

Small amounts of Fe and Si are usually present in commercial 1xxx Al alloys, either as deliberate alloying additions or as impurities. Other typical alloying or impurity elements in 1xxx Al alloys are Cu, Cr, Mn, Mg, V and Zn (Ref 1, 2), and Al-Ti-B master alloys are frequently used for grain refinement in industrial applications (Ref 3). Solute atoms are of great importance in regulating recrystallization behavior and alloy properties (Ref 4). On the other hand, with different composition and cooling rates, a wide range of Al-Fe and Al-Fe-Si intermetallic phases can form in commercial 1xxx Al alloys, among which the most typical equilibrium phases are  $\theta$ -Al<sub>13</sub>Fe<sub>4</sub> (Ref 1),  $\alpha$ -AlFeSi (Ref 5) and  $\beta$ -AlFeSi (Ref 1). Gholamali (Ref 6) investigated the effects of different Fe-Si ratios and cooling rates on the solidification of Al-Mg-Si-Fe melts. The results indicate that lower Fe-Si ratios and slower cooling rates favor the formation of the  $\beta$ -AlFeSi phase. The type, size, and distribution of the intermetallic particles have a critical influence on subsequent behaviors, such as recovery and recrystallization (Ref 7), as well as a variety of properties, including strength, toughness, plasticity, fatigue, and corrosion resistance (Ref 8).

Twin-roll casting (TRC) of 1xxx Al alloys has been widely applied due to its economic, metallurgical and environmental advantages (Ref 9, 10). Al alloys produced by TRC are expected to have refined crystallographic grains and intermetallic particles, as well as increased solid solubility (Ref 9). Since the key properties of the alloy can be regulated by both the solid solubility and the characteristics of secondary phases, which are determined by complex kinetic competition between nucleation and growth, the process–microstructure relationship is of great importance. Thermodynamic considerations often fail to correctly predict the microstructure of TRC-processed plates because of the nonequilibrium nature of solidification during twin roll casting (Ref 11). Various studies have endeavored to investigate the microstructure evolution of TRC-processed Al alloys (Ref 11, 12). The inhomogeneities of grain structure and intermetallic particles across the thickness have been observed in a variety of alloys (Ref 13), which is attributed to the temperature gradient during solidification by TRC (Ref 14). The microstructure of the TRC-processed plates can be further complicated by subsequent heat treatments (Ref 15). Due to the increased solid solubility (Ref 9), a supersaturated solid solution will form, possibly resulting in varied phase transformations. For instance, the effect of different homogenization temperatures on the intermetallic particles in an Al-1Fe-0.2Si alloy produced by TRC has been investigated by Birol (Ref 16), and the results indicate that when the Al-1Fe-0.2Si alloy is homogenized above 833 K,  $\alpha_c$  particles will be replaced by coarser Al<sub>3</sub>Fe particles.

Considering the extensive industrial application of TRC, a deeper understanding of the effects of annealing temperature and cooling rate on large Al-Fe-Si coils is of great importance. In this work, a wide variety of heat treatment parameters are applied during the recrystallization annealing of dilute Al-Fe-Si alloy plates, which are produced by TRC followed by cold-rolling. The microstructure evolution, especially that of Al-Fe-Si phases, has been investigated. The results have indicated that complex interactions have occurred between solute atoms and intermetallic particles, and the Fe-Si ratio has a great influence

**Jieke Ren**, School of Materials Science and Engineering, Zhejiang University, Hangzhou 310027, China; and Yongjie Co. Ltd., Hangzhou 311222, China; **Xiaoyang Fang**, Centre for X-mechanics, School of Aeronautics and Astronautics, Zhejiang University, Hangzhou 310027, China; **Dengbin Chen**, **Cheng Cao**, and **Youwei He**, Yongjie Co. Ltd., Hangzhou 311222, China; and **Jiabin Liu**, School of Materials Science and Engineering, Zhejiang University, Hangzhou 310027, China. Contact e-mail: liujiabin@zju.edu.cn.

on the microstructure evolution. This may shed light on the composition design of TRC-processed dilute Al-Fe-Si alloys.

## 2. Experimental

Investigations were performed on 1xxx aluminum alloys, the chemical compositions (wt.%) of which are shown in Table 1. The Fe-Si ratio of Alloy 1 was set to be lower than that of Alloy 2, to investigate the effect of the Fe-Si ratio on the properties and microstructure of Al-Fe-Si alloys. The Fe-Si weight ratio of Alloy 1 exceeds those of the common AlFeSi intermetallics, providing excess Si solute atoms, while the Fe-Si weight ratio of Alloy 2 is corresponding to that of the  $\beta$ -AlFeSi phase. Cu is added to improve the tensile strength via its significant solid solution strengthening effect, while Ti is added in the form of an Al-5Ti-1B alloy grain refiner. The overall chemical concentrations of the alloys were determined using an ARL 3460 Advantage spectrometer.

The alloys were in the form of 7-mm-thick twin-roll cast plates. Similar TRC parameters were employed in both alloys. The plates were cold-rolled (CR) to 2.5 mm sheets in 3 passes and then annealed. Considering the industrial availability of the results, where both the heating and cooling of large coils are relatively slow (generally taking several hours), the average furnace heating rate was set to be 1 K/min; the furnace temperature was maintained for 3 hours after the annealing temperature was reached, and the samples were subsequently cooled either with the furnace or in ambient air, so as to investigate the effect of the cooling rate on the microstructural evolution. The average rate of furnace cooling (FC) is estimated to be 1K/min, while the average rate of air cooling (AC) is estimated to be 50 K/min. Annealing temperatures ranging from 340 to 420 °C were used, and the temperature interval of the tests was 20 degrees. Some representative heat treatment routes selected from the heat treatment experiments are listed in Table 2, and typical curves of temperature versus time are shown in Fig. 1. The air cooling treatment corresponds to A1-T4 and A2-T4, while the furnace cooling treatment corresponds to A1-T5 and A2-T5.

The tensile mechanical properties were assessed using tensile specimens manufactured along the rolling direction. These uniaxial tensile samples possessed dimensions consistent with ASTM E8/E8M-16a, with a gauge length of 50 mm and a rectangular gauge cross-section. All tensile tests were performed using an electronic tensile testing machine at room temperature with an initial strain rate of  $3.3 \times 10^{-3}$ /s. Three parallel samples were tested for each data point, and the magnitudes of the error bars represent the standard deviations around the mean.

Optical microscopy (OM) was performed on a Zeiss AX-10 metallographic microscope. For the equiaxed grains, the grain

**Table 1 The measured chemical concentrations of the Al-Fe-Si alloys (wt.%)**

Designation	Fe	Si	Cu	Ti	Al	Fe-Si ratio
Alloy 1	0.36	0.4	0.09	0.015	Bal.	0.9
Alloy 2	0.44	0.24	0.09	0.015	Bal.	1.8

size was taken as the average of the grain boundary distance measured for each individual grain along two perpendicular lines. Scanning electron microscopy (SEM) observations were performed on an FEI Quanta FEG 650 microscope equipped with an EDAX Octane SDD energy-dispersive spectroscopy (EDS) system. The EDS electron beam diameter was 1  $\mu$ m, and for each reading a point count of 60 s was used. At least 5 particles were measured for each temper to determine the Fe-Si ratio. Samples for OM/SEM were polished both mechanically and electrolytically, using conventional techniques. Transmission electron microscopy (TEM) observations were performed on a JEOL 2100 microscope. The samples used for TEM observations were 3-mm-diameter disks that were twin-jet electropolished using standard techniques (Ref 17). Most of the bright field (BF) images were recorded near specific zone axes as indicated by the selected area electron diffraction (SAED) patterns of the FCC Al-solid solution.

**Table 2 The heat treatment routes of the Al-Fe-Si alloys**

Designation	Heat treatments	Alloy
A1-T1	As TRC plate	Alloy 1
A1-T2	As CR sheet	Alloy 1
A1-T3	Heated up to 340 °C, air cooling	Alloy 1
A1-T4	Heated up to 420 °C, air cooling	Alloy 1
A1-T5	Heated up to 420 °C, furnace cooling	Alloy 1
A2-T1	As TRC plate	Alloy 2
A2-T2	As CR sheet	Alloy 2
A2-T3	Heated up to 340 °C, air cooling	Alloy 2
A2-T4	Heated up to 420 °C, air cooling	Alloy 2
A2-T5	Heated up to 420 °C, furnace cooling	Alloy 2

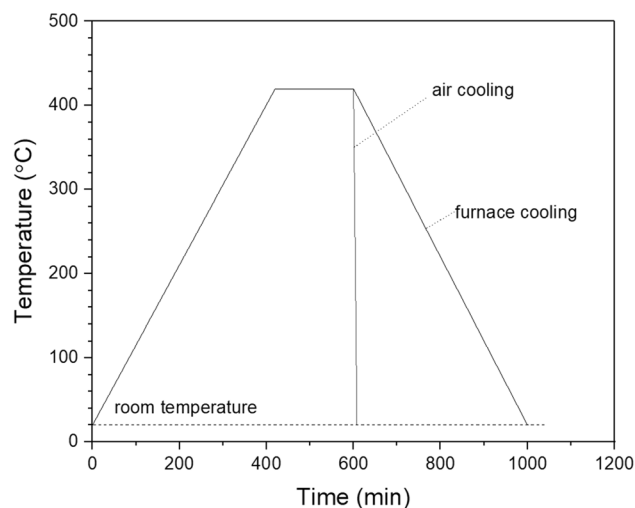


**Fig. 1** Typical annealing temperature vs. time curves

### 3. Results and Discussion

#### 3.1 OM Analysis

Figure 2 shows that for as-cast Alloy 1, significant microstructural inhomogeneity exists throughout the thickness. The difference in the grain and intermetallic particle morphologies can be attributed to the cooling rate gradient across the thickness (Ref 14). In the surface layer, which is in direct contact with the casting rolls, a higher cooling rate can be achieved, resulting in greater supercooling and a higher nucleation rate, whereas the cooling rate is relatively lower in the center layer (Ref 14). The grains are elongated in the rolling direction both on the surface and in the center, which can be attributed to plastic deformation during TRC. A continuous distribution of intermetallic phases is formed in the center layer, which is the last zone to solidify. In addition to the lower cooling rate, the low equilibrium solute partition coefficients of Fe and Si also played a part in the formation of continuous intermetallic phases (Ref 18). The concentration of Fe and Si will greatly increase in the center, as described in the Scheil equation:

$$C_s = C_0 K (1 - f_s)^{K-1} \quad (\text{Eq 1})$$

where  $C_s$  is the elemental composition of the last solidified solid,  $C_0$  is the initial elemental composition,  $K$  is the

equilibrium solute partition coefficient, and  $f_s$  is the already solidified weight fraction (Ref 19). Since the equilibrium partition coefficients of Fe and Si are below unity, the solutes will segregate to the center. The equilibrium partition coefficient of Fe (0.022) is considerably lower than that of Si (0.14) (Ref 18); thus, Fe segregation in the center is more severe, and Fe-rich particles may be formed. The OM micrographs of TRC-processed Alloy 2 resemble those of Alloy 1; thus, they are not presented here.

The morphology of CR-processed Alloy 1 is depicted in Fig. 3, whereas the structure of CR-processed Alloy 2 is omitted due to their resemblance. The deformed grains are dramatically elongated; however, the continuous intermetallic phases are only slightly fragmented during cold deformation.

To illustrate the effect of temperature on the microstructure of Al-Fe-Si alloys, the average grain size, maximum intermetallic size and intermetallic number density versus annealing temperature are depicted in Fig. 4, where only the maximum size of intermetallic particles and intermetallic number density in the surface layer are accounted for to distinguish them from the elongated intermetallic phases in the center layer formed during the TRC process. Although OM was performed for all the temperatures listed in Fig. 4, only typical micrographs of the microstructure are presented for the sake of brevity. The values of the error bars are the standard deviation of at least 3 measured areas. Fig. 4(a) shows that the grain sizes in Alloy 1

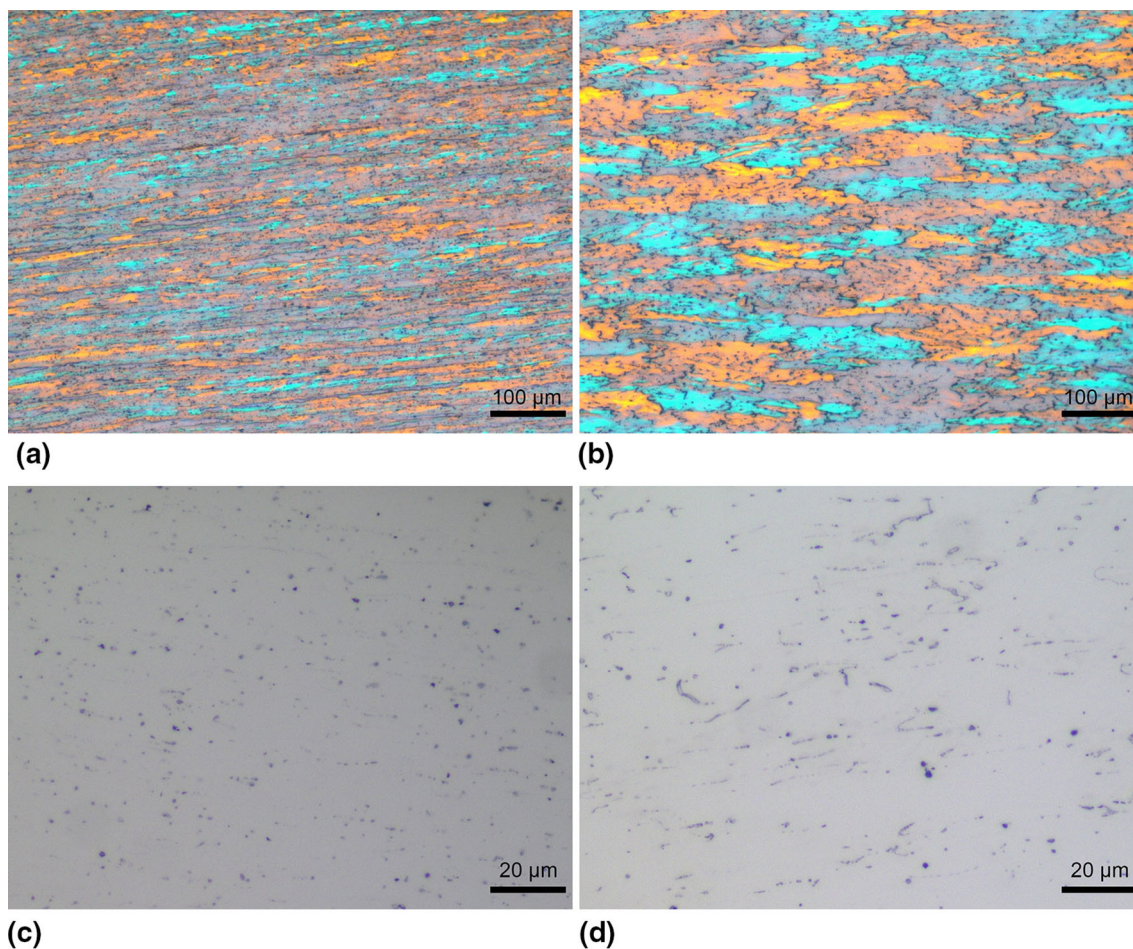


**Fig. 2** The Microstructure of TRC plate of Alloy 1: (a) grain structure near the surface, 100X; (b) grain structure in the centre, 100X; (c) intermetallic particles near the surface, 500X; (d) intermetallic particles in the centre, 500X

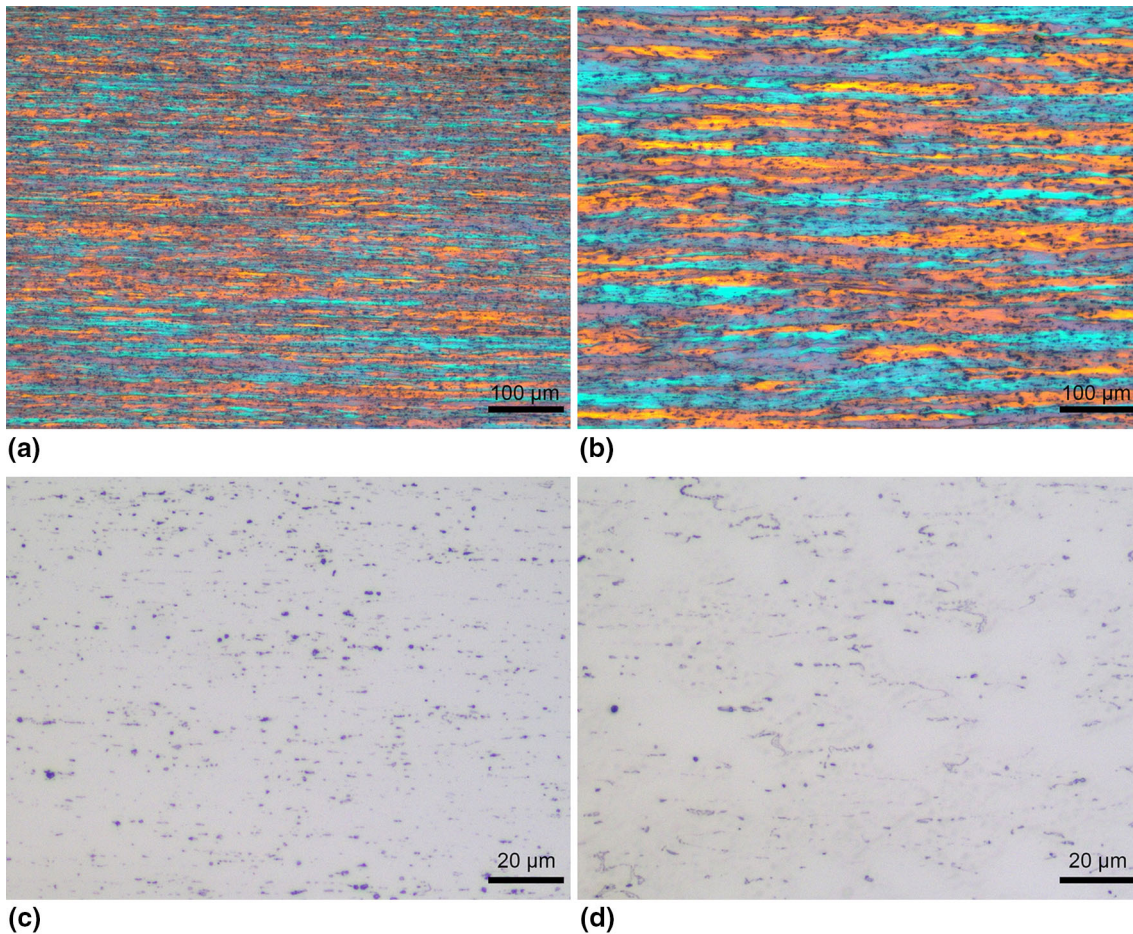


**Fig. 3** The microstructure of cold rolled sheet of Alloy 1: (a) grain structure near the surface, 100X; (b) grain structure in centre, 100X; (c) intermetallic particles near the surface, 500X; (d) intermetallic particles in centre, 500X

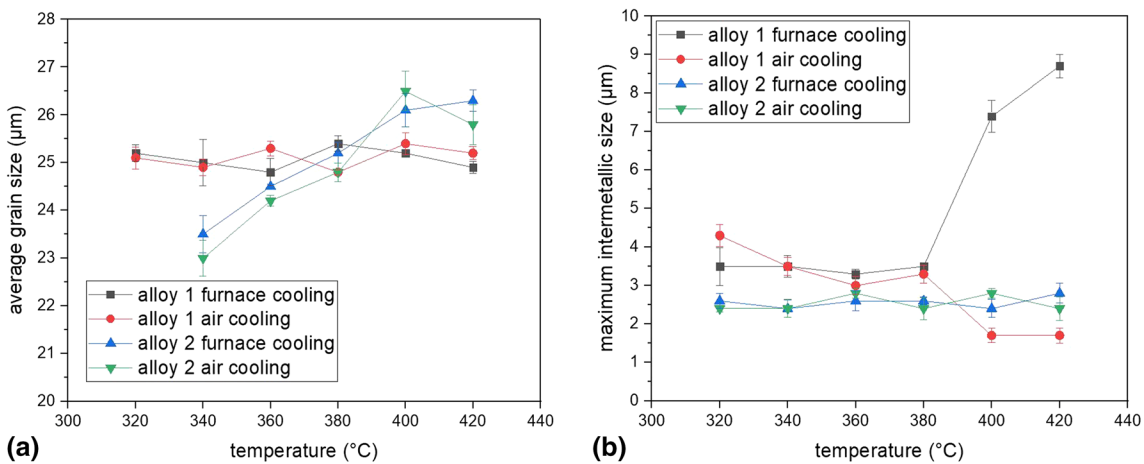


**Fig. 4** The effect of annealing temperature on the microstructure of cold rolled Al-Fe-Si alloys: (a) average grain size; (b) maximum intermetallic size

remain stable at different temperatures, indicating that no obvious grain growth occurred at the elevated annealing temperature. In Alloy 2, slight growth of grains can be observed at elevated temperatures. The different cooling methods have no obvious effect on the grain sizes, indicating that no grain growth occurred during the cooling stage. However, the intermetallic particles in Alloy 1 were moderately

refined after annealing at elevated temperature and air cooling. It can be inferred that this is due to the partial dissolution of the particles, or the decomposition of Si-rich phases, which would be accompanied by an increase in the solubility of Si atoms. The decomposition of Si-rich phases is a more reasonable explanation since Si-rich phases such as the  $\beta$ -Al<sub>5</sub>FeSi are known to be unstable under elevated temperatures (Ref 20, 21).

The Si solute atoms can pin the movement of grain boundaries, inhibiting the grain growth of Alloy 1 at elevated temperatures. On the other hand, the slight grain growth in Alloy 2 can be attributed to the lower Si concentration (fewer Si solute atoms).

The representative recrystallized microstructure of Alloy 1 is shown in Fig. 5 for visual observation. Only the grain sizes of completely recrystallized tempers are evaluated. The recrystallization temperature of 1100 alloy usually ranges from 290 to 380 °C, depending on plastic strain. In this work, after a 64.3%

thickness reduction with cold rolling, complete recrystallization took place after annealing in alloy 1 and alloy 2 at 320 °C and 340 °C, respectively, where uniform equiaxed grains were formed. This indicates that in TRC-processed alloy with a higher Si concentration (Alloy 1) the recrystallization temperature is lower. This can be attributed to the interactions between dislocations and Si solute atoms (Ref 22) during cold rolling, which resulted in increased strain energy and recrystallization driving force (Ref 23).

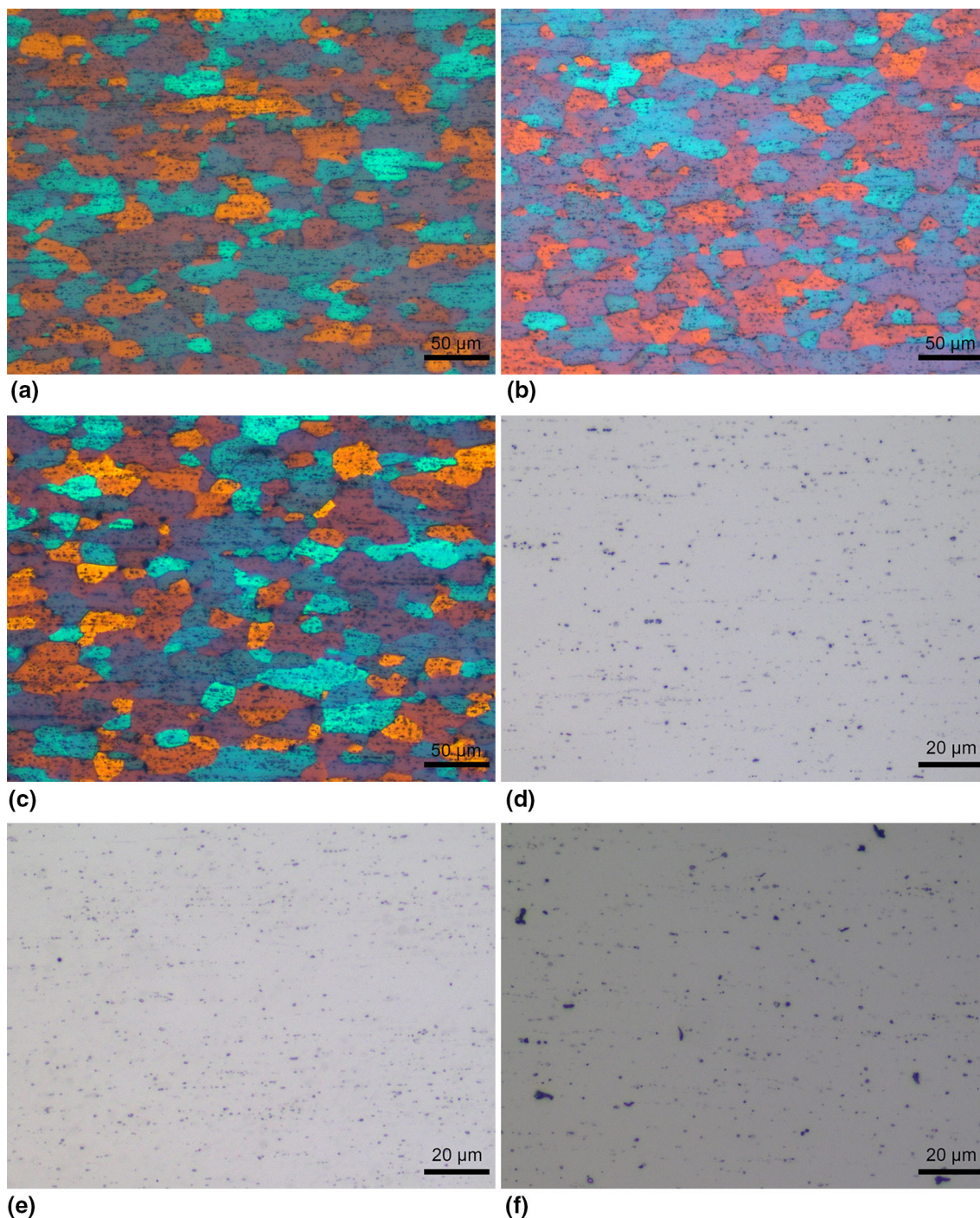


**Fig. 5** The typical recrystallized microstructure of Alloy 1 after recrystallization: (a) grain structure, A1-T3, 200X; (b) grain structure, A1-T4, 200X; (c) grain structure, A1-T5, 200X; (d) intermetallic particles, A1-T3, 500X; (e) intermetallic particles, A1-T4, 500X; (f) intermetallic particles, A1-T5, 500X

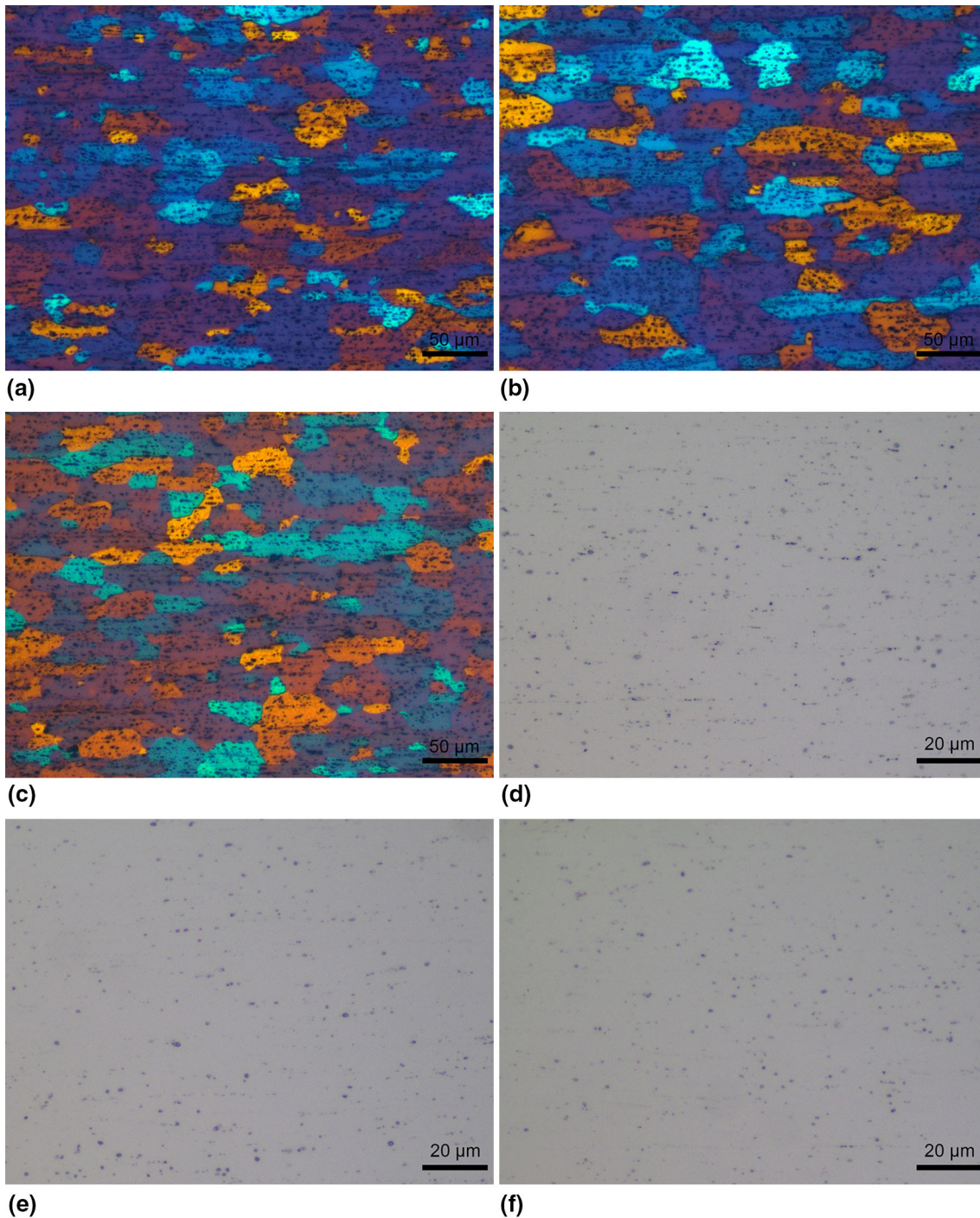


**Fig. 6** The typical intermetallic particles of Alloy 2 after recrystallization: (a) grain structure, A2-T3, 200X; (b) grain structure, A2-T4, 200X; (c) grain structure, A2-T5, 200X; (d) intermetallic particles, A2-T3, 500X; (e) intermetallic particles, A2-T4, 500X; (f) intermetallic particles, A2-T5, 500X

It is noteworthy in Fig. 4(b), Fig. 5(f) that some intermetallic particles in Alloy 1 are obviously coarsened when both elevated annealing temperatures ( $\geq 400$  °C) and furnace cooling are employed, which implies that coarsening can only occur after the particles are refined and the solubility increases at elevated annealing temperatures. It can also be inferred that coarsening took place during the slow cooling period (furnace cooling) at a temperature range below 400 °C since no coarsening is observed during annealing at temperatures above 400 °C if

air cooling is applied, as in A1-T4. The cause of coarsening is either the growth of intermetallics, or the transformation of Si-lean phases into Si-rich phases, which would be the reverse effect of the fore-mentioned decomposition of Si-rich phases. The grain sizes are not obviously affected by the evolution of intermetallic particles, as the recrystallization has been completed when heated to 340 °C, before the temperature corresponding to intermetallic particle refinement is reached, while the coarsening of intermetallic particles only occurred

during the cooling stage, thus not affecting the recrystallized grain structure.

Some typical intermetallic particles of Alloy 2 processed by different heat treatments are presented in Fig. 6.

No obvious refinement or coarsening of intermetallic particles can be observed in Alloy 2 when different annealing routes are applied. This indicates that the varied microstructural evolution of Al-Fe-Si alloys with different Fe-Si ratios is caused by the differences in the solute atom levels and/or intermetallic phase compositions, and the phases in the TRC-processed Fe-rich alloys may be more thermally stable. As a

**Table 3 Tensile mechanical properties of Al-Fe-Si alloys in different tempers**

Temper	YS, MPa	UTS, MPa	Elongation, %
1 (TRC plate, alloy 1)	85±0.6	128±0.7	23.5±1.3
2 (TRC plate, alloy 2)	86±0.6	124±0.9	21.1±1.3
3 (CR sheet, alloy 1)	173±1.2	181±0.8	7.2±0.2
4 (CR sheet, alloy 2)	161±2.0	171±2.1	6.4±0.4
5 (340 °C AC, alloy 1)	32±1.0	101±2.3	43.1±1.7
6 (420 °C AC, alloy 1)	33±2.0	104±1.0	42.7±1.7
7 (420 °C FC, alloy 1)	29±1.8	95±1.8	35.2±1.1
8 (340 °C AC, alloy 2)	33±2.1	93±2.4	38.5±1.9
9 (420 °C AC, alloy 2)	33±1.6	95±1.1	37.8±1.3
10 (420 °C FC, alloy 2)	32±2.3	92±1.9	34.7±2.4

result, an optimized Fe-Si ratio should be selected based on the specific application conditions. For example, if high toughness or damage resistance is required, the stress concentration correlated to coarse secondary phases should be avoided; thus, an Fe-Si ratio of 2 is appropriate. On the other hand, coarser intermetallics in alloys with an Fe-Si ratio of 1 might prove useful in promoting particle stimulated nucleation (PSN) during subsequent annealing. The type and composition of the intermetallic particles will be further discussed in the following sections (see parts 3.3 and 3.4).

### 3.2 Tensile Properties and Analysis

The tensile mechanical properties of the Al-Fe-Si alloys processed via different heat treatment schedules are summarized in Table 3.

The yield strength (YS) and ultimate tensile strength (UTS) of the as-cast alloys (A1-T1 and A2-T1) are higher than those of the fully recrystallized alloys, indicating that tensile deformation and strain hardening took place during TRC. The UTS of Alloy 1 (A1-T1 and A1-T2) is slightly higher than that of Alloy 2 (A2-T1 and A2-T2) due to the higher Si concentration, which would result in increased interactions between dislocations and Si solute atoms. The solution strengthening of Fe atoms can be omitted since the solubility of Fe is extremely low (0.05 wt.% at the eutectic temperature, negligible at room temperature) (Ref 18). The results indicate that the UTS of Alloy 1 increases by approximately 3 MPa after annealing at an elevated temperature (420 °C) with air cooling,

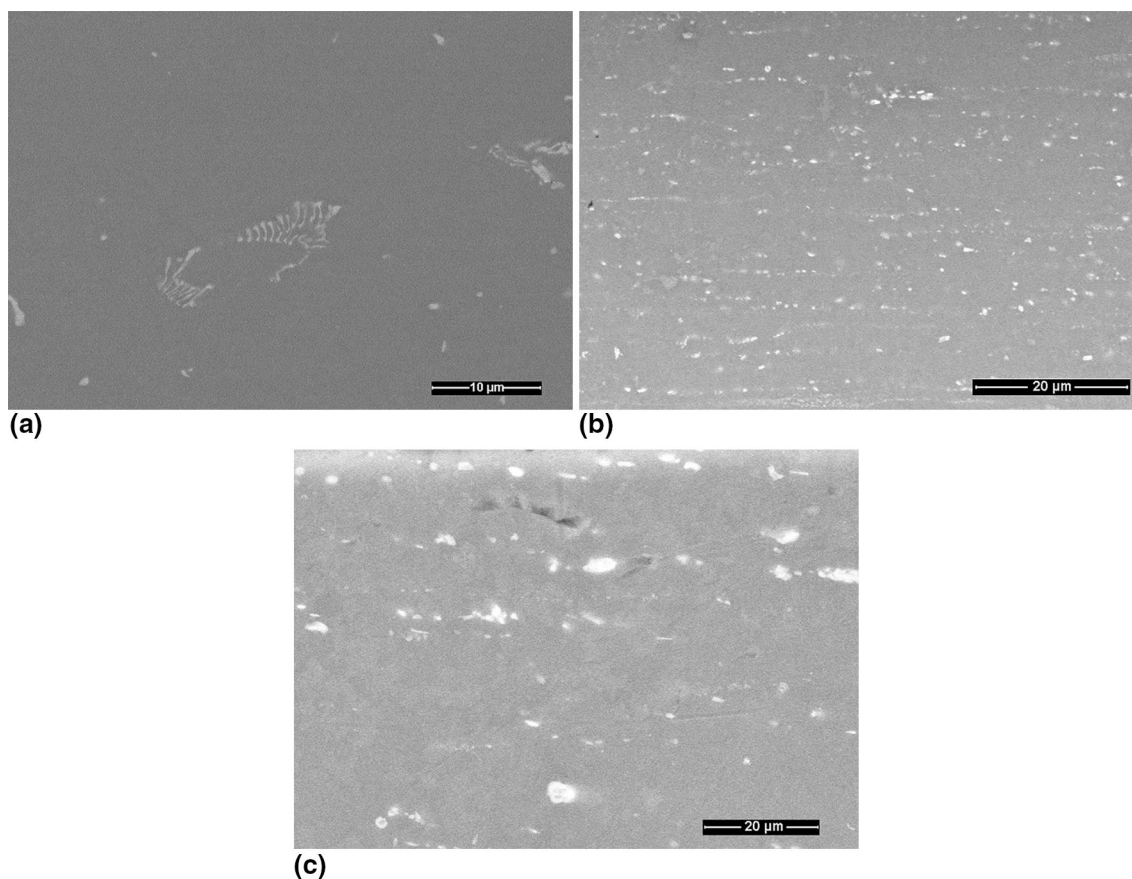


**Fig. 7** Typical intermetallic morphologies and corresponding EDS results in Al-Fe-Si alloys: (a) The eutectic-like particles in the centre layer in A1-T1; (b) The fine globular particles in the surface layer in A1-T4; (c) The coarsened particles in the surface layer in A1-T5

**Table 4 The Fe-Si ratio in different tempers**

Alloy	Temper	Morphology	Detected Fe-Si ratio	Estimated type
1	1, 4 and 5	Fine	0.9–1.2	$\beta$ -Al <sub>5</sub> FeSi (Ref 1)
1	1, 4 and 5	Fine, eutectic	2.8–3.2	$\alpha_c$ -Al <sub>12</sub> Fe <sub>3</sub> Si (Ref 27)
1	1, 4 and 5	Eutectic	3.8–4.2	$\alpha''$ -Al <sub>20</sub> Fe <sub>4</sub> Si (Ref 24)
1	1 and 4	Fine	1.8–2.2	$\alpha'$ -Al <sub>8</sub> Fe <sub>2</sub> Si (Ref 5)
1	5	Fine, coarsened	1.8–2.2	$\alpha'$ -Al <sub>8</sub> Fe <sub>2</sub> Si
2	1, 4 and 5	Fine	0.9–1.2	$\beta$ -Al <sub>5</sub> FeSi
2	1, 4 and 5	Fine, eutectic	2.8–3.2	$\alpha_c$ -Al <sub>12</sub> Fe <sub>3</sub> Si
2	1, 4 and 5	Fine	1.4–1.6, 1.8–2.2	$\alpha'$ -Al <sub>8</sub> Fe <sub>2</sub> Si or Al <sub>12</sub> Fe <sub>3</sub> Si <sub>2</sub>

and the changes in tensile strength are attributed to the increase in Si solubility during the refinement of intermetallic particles, which is consistent with the OM observations. When furnace cooling is applied in 420 °C annealing, a 9 MPa decrease in tensile strength can be observed. This can be attributed to the coarsening of intermetallic particles, accompanied by a decrease in solution strengthening. The elongation value of A1-T4 is also decreased by 7.5%. This may be attributed to strain localization at the interfaces between the matrix and coarse intermetallic particles. In Alloy 2, an increase of 2 MPa in tensile strength is also observed. However, the decrease in tensile strength is only 3 MPa when furnace cooling is applied, which is obviously less than the decrease in the tensile strength of Alloy 1.

### 3.3 SEM Analysis

Conventionally, the Al-Fe-Si phases in direct-chill cast alloys can be identified based on morphology and semiquantitative compositional analysis (Ref 18). However, in TRC-processed alloys, the morphologies of the intermetallic phases are greatly influenced by the cooling rate gradient during TRC, as shown in Fig. 2; thus, identification based on the morphologies is not applicable. Some typical intermetallic morphologies are shown in Fig. 7, while the Fe-Si ratios of intermetallic phases with different morphologies are listed in Table 4. Note that since the electron beam diameter is 1  $\mu$ m when analyzing the composition of a small particle, some signal may be collected from the matrix, resulting in high Al concentrations; thus, the absolute composition values are not listed.

The Fe-Si ratio results in Table 4 indicate that certain types of Al-Fe-Si phases exist in different tempers of both alloys, which are estimated to be  $\beta$ -AlFeSi,  $\alpha_c$ -Al<sub>12</sub>Fe<sub>3</sub>Si and  $\alpha'$ -Al<sub>8</sub>Fe<sub>2</sub>Si (or Al<sub>12</sub>Fe<sub>3</sub>Si<sub>2</sub>). The eutectic phases in the center layer are estimated to be  $\alpha_c$ -Al<sub>12</sub>Fe<sub>3</sub>Si and  $\alpha''$ -Al<sub>20</sub>Fe<sub>4</sub>Si in Alloy 1, while only the  $\alpha_c$ -Al<sub>12</sub>Fe<sub>3</sub>Si phase can be observed in Alloy 2. It can be inferred that the formation of the eutectic phase with a higher Fe concentration is facilitated by the segregation of Fe atoms in the center layer, whereas the  $\alpha''$ -Al<sub>20</sub>Fe<sub>4</sub>Si phase is a low Si modification of  $\alpha$ -AlFeSi phase (Ref 24). However, it is intriguing that Fe-rich  $\alpha''$ -Al<sub>20</sub>Fe<sub>4</sub>Si can only be observed in Alloy 1, while the Si rich variant of  $\alpha'$ -Al<sub>12</sub>Fe<sub>3</sub>Si<sub>2</sub> can only be observed in Fe-rich Alloy 2. Although the formation of  $\beta$ -Al<sub>5</sub>FeSi is generally considered to be inhibited at high cooling rates,  $\beta$ -Al<sub>5</sub>FeSi can still be observed in both TRC-processed alloys. The Fe-Si ratios of the coarsened intermetallics of A1-T5 are in agreement with those of  $\alpha'$ -Al<sub>8</sub>Fe<sub>2</sub>Si. This ternary phase is considered to be the equilibrium phase in dilute AlFeSi alloys and more thermodynamically stable at elevated temperatures, which can be

observed even after long periods of homogenization (Ref 1).  $\beta$ -Al<sub>5</sub>FeSi can transform into  $\alpha'$ -Al<sub>8</sub>Fe<sub>2</sub>Si during homogenization (Ref 5). However, it is unclear whether coarsening occurs merely by the preferential growth of existing  $\alpha'$ -Al<sub>8</sub>Fe<sub>2</sub>Si or the transformation from  $\beta$ -Al<sub>5</sub>FeSi to  $\alpha'$ -Al<sub>8</sub>Fe<sub>2</sub>Si, as all three types of AlFeSi phases coexist before or after different annealing schedules are applied to TRC-processed Alloy 1. Since the refinement of intermetallics is required for the subsequent growth of the coarsened phases, the solute atoms probably played a vital part in coarsening, and the growth mechanism is inferred to be via uphill diffusion, which occurred during the cooling stage below 400 °C. The Fe-Si ratios and morphology of intermetallics remain unchanged in different tempers of Alloy 2 even though the types of intermetallics are mostly similar, confirming that the refinement of intermetallics played a part in the coarsening of the  $\alpha'$ -Al<sub>8</sub>Fe<sub>2</sub>Si phase in Alloy 1.

### 3.4 TEM Analysis

Representative TEM micrographs and corresponding SAED patterns recorded for different tempers of Alloy 1 are provided in Fig. 7. A high density of entangled dislocations can be observed in the cold-rolled state, as shown in Fig. 8(a). Entangled dislocations can be observed near the intermetallic particle in Fig. 8(b). The dislocations formed subgrain boundaries or cell walls after annealing, as shown in Fig. 8(c). Based on the extra spots in the diffraction pattern of the Al matrix ( $\langle 110 \rangle_{\alpha\text{-Al}}$ ) in Fig. 8(a), the fine intermetallics are identified as the  $\beta$ -Al<sub>5</sub>FeSi phase. This phase has a monoclinic structure with  $a = 0.6161$  nm,  $b = 0.6175$  nm,  $c = 2.0813$  nm, and  $\beta = 90.42^\circ$  (Ref 25). The intermetallics observed in Fig. 8(b) are identified as the bcc  $\alpha_c$ -Al<sub>12</sub>Fe<sub>3</sub>Si phase based on the diffraction pattern of the  $\langle 110 \rangle_{\text{bcc}}$  zone axis. The  $\alpha_c$ -AlFeSi phase has a bcc structure with  $a = 1.256$  nm (Ref 26). The intermetallics observed in Fig. 8(c) are identified as the hexagonal  $\alpha'$ -Al<sub>8</sub>Fe<sub>2</sub>Si phase ( $a = b = 1.23$  nm,  $c = 2.62$  nm) (Ref 1) based on the diffraction pattern in the  $\langle 072 \rangle$  direction. However, so far, only these 3 types of AlFeSi phases have been confirmed by the SAED method, verifying the presence of the other phases such as Al<sub>20</sub>Fe<sub>4</sub>Si still needs further investigation.

## 4. Conclusions

In twin-roll cast dilute AlFeSi alloys, different morphologies and types of intermetallic phases are formed across the thickness. Fine spherical  $\beta$ -AlFeSi,  $\alpha_c$ -Al<sub>12</sub>Fe<sub>3</sub>Si and  $\alpha'$ -Al<sub>8</sub>Fe<sub>2</sub>Si phases coexist. Eutectic  $\alpha_c$ -Al<sub>12</sub>Fe<sub>3</sub>Si can be observed



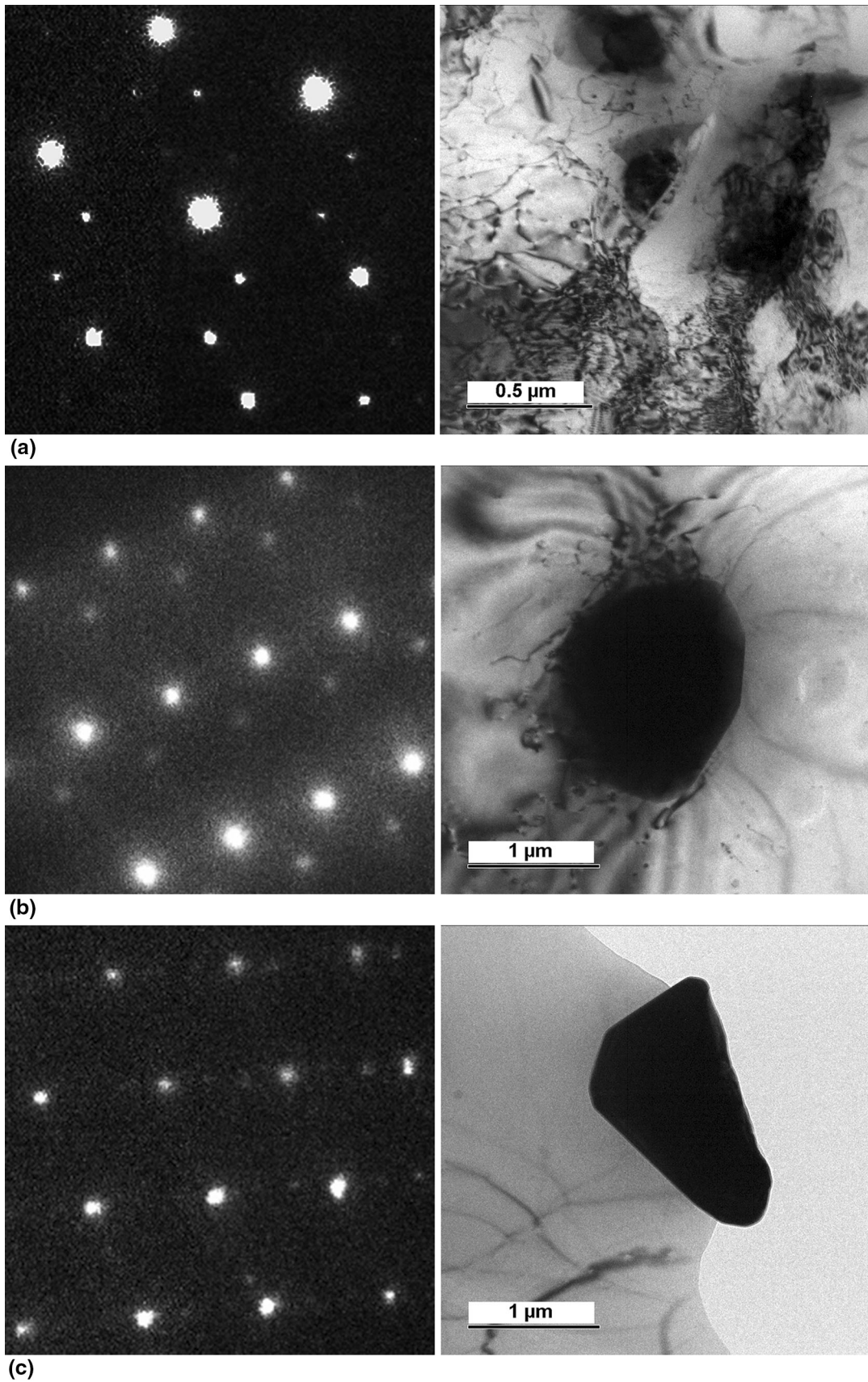


**Fig. 8** The bright field TEM micrographs and SAED patterns in Al-Fe-Si alloys: (a)  $\beta$ - $\text{Al}_5\text{FeSi}$  phase in Al-T2, recorded near  $\langle 110 \rangle_{\alpha\text{-Al}}$ ; (b)  $\alpha_c$ - $\text{Al}_{12}\text{Fe}_3\text{Si}$  phase in Al-T4, recorded near  $\langle 110 \rangle_{\text{bcc}}$ ; (c)  $\alpha'$ - $\text{Al}_8\text{Fe}_2\text{Si}$  phase in Al-T5 in  $\langle 072 \rangle$  direction

due to the higher Fe concentration in the center layer. In a twin-roll cast Al-0.36Fe-0.4Si alloy, annealing at elevated temperatures ( $\geq 400$  °C) would lead to a slight refinement of intermetallic particles. During a slow cooling period (furnace cooling), the coarsening of the  $\alpha'$ -Al<sub>8</sub>Fe<sub>2</sub>Si phase occurred below 400 °C after the refinement of the intermetallic particles. The recrystallized grain size is not obviously affected by the evolution of intermetallic phases, as recrystallization completed before the evolution of intermetallic phases took place. The morphologies and types of intermetallic phases in the twin-roll cast Al-0.44Fe-0.24Si alloy are unaffected by the heat treatments despite the similarity in the intermetallic types, indicating that the refinement of intermetallics is essential for coarsening to occur. As a result, for twin-roll cast Al-Fe-Si alloys with a low Fe-Si ratio ( $\sim 1$ ), a low annealing temperature or rapid cooling should be applied if the coarsening of intermetallics is to be avoided.

## Funding

This work was supported by Fundamental Research Funds for the Central Universities (2018XZZX001-05).

## References

1. C.M. Allen, K.A.Q. O'Reilly, B. Cantor, and P.V. Evans, Intermetallic Phase Selection in xxx Al Alloys, *Prog. Mater. Sci.*, 1998, **43**(2), p 89–170
2. M. Shakiba, N. Parson, and X.-G. Chen, Hot Deformation Behavior and Rate-Controlling Mechanism in Dilute Al-Fe-Si Alloys with Minor Additions of Mn and Cu, *Mater. Sci. Eng. A*, 2015, **636**, p 572–581
3. C.M. Allen, K.A.Q. O'Reilly, P.V. Evans, and B. Cantor, The Effect of Vanadium and Grain Refiner Additions on the Nucleation of Secondary Phases in xxx Al Alloys, *Acta Mater.*, 1999, **47**(17), p 4387–4403
4. R.K. Davies, V. Randle, and G.J. Marshall, Continuous Recrystallization—Related Phenomena in a Commercial Al-Fe-Si Alloy, *Acta Mater.*, 1998, **46**(17), p 6021–6032
5. H. Tanihata, T. Sugawara, K. Matsuda, and S. Ikeno, Effect of Casting and Homogenizing Treatment Conditions on the Formation of Al-Fe-Si Intermetallic Compounds in 6063 Al-Mg-Si Alloys, *J. Mater. Sci.*, 1999, **34**(6), p 1205–1210
6. F.C.M. Gholamali, Les effets des éléments de trace sur les caractéristiques des alliages de type 6xxx pour les applications automobiles, Université du Québec à Chicoutimi, 1999, p 14–85
7. Y. Birol, Effect of Homogenization on Recrystallization in a Twin-Roll Cast Al-Fe-Si Alloy, *J. Mater. Sci.*, 2008, **43**(13), p 4652–4657
8. T. Turmezey, AlFe and AlFeSi Intermetallic Phases in Aluminium Alloys, *Mater. Sci. Forum*, 1987, **13**, p 121–132
9. N.S. Barekar and B.K. Dhindaw, Twin-Roll Casting of Aluminum Alloys—an Overview, *Mater. Manuf. Process*, 2014, **29**(6), p 651–661
10. T. Haga, K. Tkahashi, M. Ikawaand, and H. Watari, Twin Roll Casting of Aluminum Alloy Strips, *J. Mater. Process Technol.*, 2004, **153**, p 42–47
11. S. Kumar, N. Hari Babu, G.M. Scamans, and Z. Fan, Microstructural Evaluation of Melt Conditioned Twin Roll Cast Al-Mg Alloy, *Mater. Sci. Tech.*, 2011, **27**(12), p 1833–1839
12. M. Yun, S. Loky, and J.D. Hunt, Twin Roll Casting of Aluminium Alloys, *Mater. Sci. Eng. A*, 2000, **280**(1), p 116–123
13. M. Šlapáková, M. Zimina, S. Zaunschirm, J. Kastner, J. Bajer, and M. Cieslar, 3D Analysis of Macrosegregation in Twin-Roll Cast AA3003 Alloy, *Mater. Charact.*, 2016, **118**, p 44–49
14. B.S. Berg, V. Hansen, P.T. Zagiarski, M.L. Nedreberg, A. Olsen, and J. Gjønnnes, Gauge Reduction in Twin-Roll Casting of an Aa5052 Aluminium Alloy: The Effects on Microstructure, *J. Mater. Process Technol.*, 1995, **53**(1–2), p 65–74
15. O. Grydin, M. Schaper, and V. Danchenko, Twin-Roll Casting of High-strength Age-hardened Aluminium Alloys, *Metall. Min. Ind.*, 2011, **3**(7), p 7–16
16. Y. Birol, Thermomechanical Processing of a Twin-Roll Cast Al-1Fe-0.2Si Alloy, *J. Mater. Process Technol.*, 2008, **202**(1), p 564–568
17. D.B. Williams and C.B. Carter, *Transmission Electron Microscopy: A Textbook for Materials Science*, Plenum Press, New York, 2009, p 173–194
18. W. Khalifa, F.H. Samuel, and J.E. Gruzleski, Iron Intermetallic Phases in the Al Corner of the Al-Si-Fe System, *Metall. Mater. Trans. A*, 2003, **34**(3), p 807–825
19. E.D.S. Meza, F. Bertelli, P.R. Goulart, N. Cheung, and A. Garcia, The Effect of the Growth Rate on Microsegregation: Experimental Investigation in Hypoeutectic Al-Fe and Al-Cu Alloys Directionally Solidified, *J. Alloy. Compd.*, 2013, **561**, p 193–200
20. M. Wang, W. Xu, and Q. Han, Effect of Heat Treatment on Controlling the Morphology of AlFeSi Phase in A380 Alloy, *Int. J. Metalcast*, 2016, **10**(4), p 516–523
21. G. Haidemenopoulos, H. Kamoutsi, and A. Zervaki, Simulation of the Transformation of Iron Intermetallics During Homogenization of 6xxx Series Extrudable Aluminum Alloys, *J. Mater. Process Technol.*, 2012, **212**(11), p 2255–2260
22. G.P.M. Leyson, W.A. Curtin, L.G. Hector, and C.F. Woodward, Quantitative Prediction of Solute Strengthening In Aluminium Alloys, *Nat. Mater.*, 2010, **9**(9), p 750–755
23. W. Blum and H. McQueen, Dynamics of Recovery and Recrystallization, *Mater. Sci. Forum*, 1996, **217**, p 31–42
24. P. Skjerpe, Intermetallic Phases Formed During DC-Casting of an Al-0.25 wt Pct Fe-0.13 wt Pct Si Alloy, *Metall. Mater. Trans. A*, 1987, **18**(2), p 189–200
25. C. Rømming, V. Hansen, and J. Gjønnnes, Crystal Structure of  $\beta$ -Al<sub>45</sub>FeSi, *Acta Crystallogr. B*, 1994, **50**(3), p 307–312
26. L. Sweet, S.-M. Zhu, S. Gao, J. Taylor, and M. Easton, The Effect of Iron Content on the Iron-Containing Intermetallic Phases in a Cast 6060 Aluminum Alloy, *Metall. Mater. Trans. A*, 2011, **42**(7), p 1737–1749
27. M.H. Mulazimoglu, A. Zaluska, J.E. Gruzleski, and F. Paray, Electron Microscope Study of Al-Fe-Si Intermetallics in 6201 Aluminum Alloy, *Metall. Mater. Trans. A*, 1996, **27**(4), p 929–936

**Publisher's Note** Springer Nature remains neutral with regard to jurisdictional claims in published maps and institutional affiliations.